MEASUREMENT OF GLOBAL SPIN ALIGNMENT OF VECTOR MESONS AT RHIC* **

Subhash Singha

for the STAR Collaboration

Institute of Modern Physics Chinese Academy of Sciences, Lanzhou, 73000, China
subhash@impcas.ac.cn

Received 1 August 2022, accepted 2 October 2022, published online 14 December 2022

We report on the measurements of spin alignment (ρ_{00}) for K^{*0}, $\overline{K^{*0}}$, K^{*+}, and K^{*-} vector mesons in the RHIC isobar collisions (Zr+Zr and Ru+Ru) at $\sqrt{s_{NN}} = 200$ GeV. We observe the first non-zero spin alignment for $K^{*\pm}$ in heavy-ion collisions. The $K^{*\pm}$ ρ_{00} is about 3.9σ larger than that of K^{*0}. The observed difference and the ordering between $K^{*\pm}$ and K^{*0} are surprising and require further inputs from theory. When comparing the isobar and Au+Au collisions, no significant system size dependence in K^{*0} ρ_{00} is observed within uncertainties.

DOI:10.5506/APhysPolBSupp.16.1-A34

1. Introduction

In the initial stage of non-central heavy-ion collisions (HIC), a large orbital angular momentum (OAM) is imparted into the system. The magnitude of such an OAM can be $\sim bA\sqrt{s_{NN}} \sim 10^4\hbar$, where b is the impact parameter and A is the mass number of the collision species [1]. Part of OAM transferred to the Quark–Gluon Plasma (QGP) medium can polarize quarks and anti-quarks due to "spin–orbit" interaction and hence induce a non-vanishing polarization for hadrons with non-zero spin [2]. The incoming charged spectators in HIC can also induce a large but short-lived magnetic field ($eB \sim 10^{18}$ Gauss) [3]. Such a strong B-field can also polarize both quarks and anti-quarks due to its coupling with the intrinsic magnetic moment. The measurement of spin polarization cannot only offer insights into the initial orbital angular momentum interactions and magnetic field, but also serve as an experimental probe to understand the response of QGP

* Presented at the 29th International Conference on Ultrarelativistic Nucleus–Nucleus Collisions: Quark Matter 2022, Kraków, Poland, 4–10 April, 2022.

** S.S. is supported by the Strategic Priority Research Program of Chinese Academy of Sciences.

medium under these extreme initial conditions. The measurement of significant non-zero polarization of Λ hyperons by the STAR Collaboration offered the first experimental evidence of the presence of vorticity of the QGP medium induced by the initial angular momentum, while a hint of difference between Λ and $\bar{\Lambda}$ spin polarization at RHIC presents an opportunity to probe the initial B-field [4].

The spin alignment is quantified by 00^{th} element of the spin density matrix, ρ_{00}, and can be measured from the angular distribution of the decay daughter of the vector meson [5]

$$\frac{\mathrm{d}\,N}{\mathrm{d}\,\cos\theta^*} \propto \left((1-\rho_{00}) + (3\rho_{00}-1)\cos^2\theta^*\right), \tag{1}$$

where θ^* is the angle between the polarization axis and momentum direction of the daughter particle in the rest frame of its parent. For global spin alignment, the polarization axis is chosen as the direction perpendicular to the reaction plane, which can be correlated with both the OAM and the B-field. The value of ρ_{00} is expected to be $\frac{1}{3}$ in the absence of spin alignment, while a deviation of ρ_{00} from $\frac{1}{3}$ indicates a net spin alignment.

At present, the available physics mechanisms that can cause spin alignment are the following: *(i)* the polarized quarks induced by vorticity can hadronize via the coalescence mechanism. It can make ρ_{00} smaller than $\frac{1}{3}$ [2, 6]; *(ii)* the ρ_{00} induced by the B-field can be either larger or smaller than $\frac{1}{3}$. The expected deviation due to vorticity and B-field is $\rho_{00}-\frac{1}{3}\sim 10^{-5}$ [6]; *(iii)* the electric field can give a positive contribution with $\rho_{00}-\frac{1}{3}\sim 10^{-4}$ [6]; *(iv)* the fragmentation of polarized quarks can make either positive or negative contribution with $\rho_{00}-\frac{1}{3}\sim 10^{-5}$ [2]; *(v)* local spin alignment, helicity polarization, and turbulent color field can also make ρ_{00} smaller than $\frac{1}{3}$ [7]; *(vi)* a fluctuating strong force field of vector meson can cause the ρ_{00} to be larger than $\frac{1}{3}$ with a deviation ~ 0.1, which is an order of magnitude larger compared to more conventional mechanisms [8]. The study of ρ_{00} of various vector meson species can thus elucidate our understanding of different mechanisms causing spin alignment. Furthermore, the neutral and charged vector mesons ($K^{*0}(d\bar{s})$ and $K^{*+}(u\bar{s})$) have similar mass, but the magnetic moments of their constituent quarks differ by about a factor of five ($\mu_d\sim -0.97\mu_{\mathrm{N}}$, $\mu_u\sim 1.85\mu_{\mathrm{N}}$). Hence, the magnetic field-driven contribution to the ρ_{00} of neutral and charged K^* is expected to be different.

The recent measurements of ρ_{00} of ϕ and K^{*0} vector mesons from the 1^{st} phase of the RHIC Beam Energy Scan (BES-I) in Au+Au collisions revealed a surprising pattern [13]. While the K^{*0} ρ_{00} is largely consistent with $\frac{1}{3}$, the ϕ mesons show a large positive deviation ($\rho_{00}>\frac{1}{3}$) with about 8.4σ significance when ρ_{00} is integrated within the range of $\sqrt{s_{NN}}=11.5$–62.4 GeV for $1.2<p_{\mathrm{T}}<5.4$ GeV/c in 20–60% Au+Au collisions. Such

a large positive deviation at mid-central collisions poses challenges to more conventional physics mechanisms, while the polarization induced from a fluctuating ϕ-meson vector field can accommodate the large positive signal [8]. Moreover, the p_{T} and centrality differential measurements of ϕ and K^{*0} ρ_{00} in the BES-I energy range also show non-trivial patterns [13].

2. Analysis method

These proceedings report on the first ρ_{00} measurements of charged $K^{*\pm}$ along with neutral K^{*0} ($\overline{K^{*0}}$) vector mesons in the RHIC isobar collisions of $^{96}_{44}$Ru+$^{96}_{44}$Ru and $^{96}_{40}$Zr+$^{96}_{40}$Zr species at $\sqrt{s_{NN}} = 200$ GeV [9]. The $K^{*0}(\overline{K^{*0}})$ and $K^{*+}(K^{*-})$ are reconstructed via $K^{*0}(\overline{K^{*0}}) \to \pi^- + K^+(\pi^+ + K^-)$ and $K^{*+}(K^{*-}) \to \pi^+ + K^0_{\mathrm{S}}(\pi^- + K^0_{\mathrm{S}})$, respectively. The minimum-bias (MB) events are collected via a coincidence between the Vertex Position Detectors (VPD) located at $4.4 < |\eta| < 4.9$. For analysis, the vertex position along the beam ($V_{z,\mathrm{TPC}}$) and radial direction (V_r) are required to be within $-35 < V_{z,\mathrm{TPC}} < 25$ cm and $V_r < 5$ cm respectively with a coordinate system at the center of Time Projection Chamber (TPC). We analyzed about 1.8 and 2.0 billion good MB events for Ru+Ru and Zr+Zr collisions, respectively. The charged particle tracking is performed using the TPC. The collision centrality is determined from the number of charged particles within $|\eta| < 0.5$ and using a Monte Carlo Glauber simulation [10]. The second-order event plane ($\Psi_{2,\mathrm{TPC}}$) is reconstructed using the tracks inside TPC [11]. In isobar collisions, the typical $\Psi_{2,\mathrm{TPC}}$ resolution achieved in mid-central collisions is $R_{2,\mathrm{TPC}} \sim 64\%$. The decay daughters of K^* are identified using the specific ionization energy loss in TPC gas volume and the velocity of particles measured by the TOF detector. The K^0_{S} mesons are selected via a weak decay topology. For charged $K^{*\pm}$ reconstruction, only the K^0_{S} candidates within $0.48 < M(\pi^+\pi^-) < 0.51$ GeV/c^2 are considered. The combinatorial background is estimated from a track rotation technique, in which one of the daughter tracks is rotated by 180° to break the correlation among the pairs originating from the same parent particle. Then, the invariant mass signal is obtained by subtracting the combinatorial background. The K^* signal is fitted with a Breit–Wigner distribution and a second-order polynomial function to take care of the residual background.

The left panel in Fig. 1 presents the K^{*+} signal for $2.0 < p_{\mathrm{T}} < 2.5$ GeV/c in 20–60% Zr+Zr collisions at $\sqrt{s_{NN}} = 200$ GeV. The yield is estimated by integrating residual background subtracted signal within the range: $m_0 \pm 3\Gamma$, where m_0 and Γ are the invariant mass peak position and width of K^*. The yield is obtained in five $|\cos\theta^*|$ bins, where θ^* is the angle between $\Psi_{2,\mathrm{TPC}}$ and momentum of daughter kaon (pion) in the parent K^{*0} ($K^{*\pm}$) rest frame. The detector acceptance and efficiency correction factors are obtained using

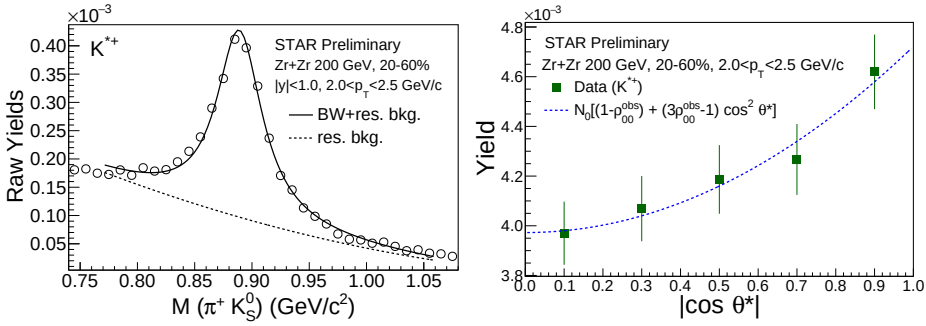

Fig. 1. Left: $K^{*+}(\rightarrow \pi^+ + K^0_S)$ invariant mass distribution for $2.0 < p_T < 2.5$ GeV/c in 20–60% Zr+Zr collisions at $\sqrt{s_{NN}} = 200$ GeV. Right: efficiency and acceptance corrected K^{*+} yield as a function of $|\cos\theta^*|$ in 200 GeV Zr+Zr collisions.

a STAR detector simulation in Geant3. The right panel in Fig. 1 presents efficiency and acceptance corrected K^{*+} yield as a function of $|\cos\theta^*|$ for $2.0 < p_T < 2.5$ GeV/c in 20–60% Zr+Zr collisions. The yield *versus* $|\cos\theta^*|$ distribution is then fitted with Eq. (1) and the extracted ρ_{00} (called $\rho_{00}^{\rm obs}$) is corrected for event plane resolution using: $\rho_{00} = \frac{1}{3} + \frac{4}{1+3R_{2,\rm TPC}}(\rho_{00}^{\rm obs} - \frac{1}{3})$ [12].

3. Results

The left panel of Fig. 2 presents the p_T dependence of ρ_{00} for K^{*0} and $\overline{K^{*0}}$ at mid-rapidity ($|y| < 1.0$) in 20–60% central Ru+Ru and Zr+Zr collisions at $\sqrt{s_{NN}} = 200$ GeV. The ρ_{00} between the particle and anti-particle species are consistent within errors. These results are compared with that from 200 GeV Au+Au collisions [13]. The ρ_{00} between isobar and Au+Au collisions are consistent within uncertainties across the measured p_T region in mid-central

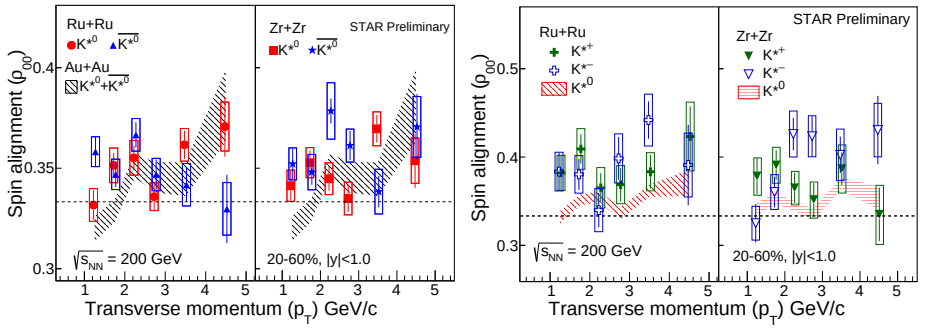

Fig. 2. Left: $\rho_{00}(p_T)$ for K^{*0} and $\overline{K^{*0}}$ in isobar collisions at $\sqrt{s_{NN}} = 200$ GeV. Results are compared with that from 200 GeV Au+Au collisions [13]. Right: comparison of $\rho_{00}(p_T)$ between $K^{*\pm}$ and K^{*0} in 200 GeV isobar collisions.

collisions. The right panel of Fig. 2 shows a comparison of $\rho_{00}(p_{\mathrm{T}})$ among neutral and charged K^* species in isobar collisions. The ρ_{00} for charged $K^{*\pm}$ are systematically larger than the neutral K^{*0} across the measured p_{T} region. The left panel of Fig. 3 presents the ρ_{00} as a function of the average number of participants ($\langle N_{\mathrm{part}}\rangle$) for K^{*0} and $\overline{K^{*0}}$ for $1.0 < p_{\mathrm{T}} < 5.0$ GeV/c in 200 GeV Ru+Ru and Zr+Zr collisions. These results are compared with that from 200 GeV Au+Au collisions [13]. The K^{*0} ρ_{00} is larger than $\frac{1}{3}$ at smaller $\langle N_{\mathrm{part}}\rangle$. It is smaller than $\frac{1}{3}$ at large $\langle N_{\mathrm{part}}\rangle$, which can have contributions from the local spin alignment [7]. At a similar $\langle N_{\mathrm{part}}\rangle$, the ρ_{00} between small system isobar and large system Au+Au are comparable within uncertainties.

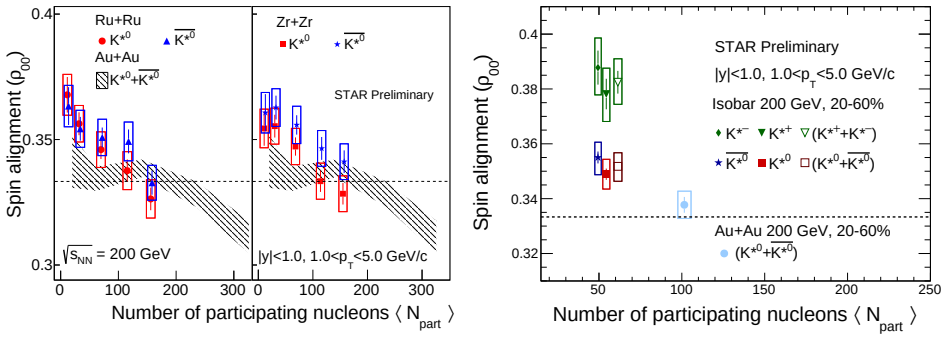

Fig. 3. Left: $\rho_{00}(\langle N_{\mathrm{part}}\rangle)$ for K^{*0} and $\overline{K^{*0}}$ in isobar collisions at $\sqrt{s_{NN}} = 200$ GeV. Right: p_{T} integrated ρ_{00} for K^{*0}, $\overline{K^{*0}}$, K^{*+}, and K^{*-} in 20–60% 200 GeV isobar collisions. Results are compared with K^{*0} in 200 GeV Au+Au collisions [13].

The right panel of Fig. 3 summarizes the p_{T}-integrated ρ_{00} for K^{*0}, $\overline{K^{*0}}$, K^{*+}, and K^{*-} in 20–60% isobar collisions. These results are compared with $(K^{*0}+\overline{K^{*0}})$ ρ_{00} from Au+Au collisions [13]. This is the first observation of $K^{*\pm}$ ρ_{00} to be larger than $\frac{1}{3}$ in heavy-ion collisions. Moreover, the p_{T}-integrated ρ_{00} reveals a clear ordering between neutral and charged K^* species in isobar collisions, with the charged species about 3.9σ larger than the neutral ones. Due to the interaction between the B-field and the magnetic moment of the constituent quarks, one naively expects the K^{*0} ρ_{00} to be larger than that of $K^{*\pm}$ [6]. However, the observed ordering between K^{*0} and $K^{*\pm}$ is opposite to such a naive expectation. Although the reason behind the difference between K^{*0} and $K^{*\pm}$ ρ_{00} is not understood yet, these species might have different contributions from the vector meson strong force field. More inputs from theory are required to better understand the underlying physics mechanisms.

4. Summary and conclusion

In summary, the measurements of ϕ and K^{*0} ρ_{00} in Au+Au collisions from RHIC BES-I reveal a surprising pattern with a large positive deviation from $\frac{1}{3}$ for ϕ mesons and no obvious deviation for K^{*0}. At present, a fluctuating vector meson strong force field can accommodate the large positive deviation for ϕ mesons, while more theory inputs are needed for K^{*0}. The recent high statistics RHIC isobar collision (Ru+Ru and Zr+Zr) data offer a new opportunity to extend the measurement of ρ_{00} for K^{*0}, $\overline{K^{*0}}$, K^{*+}, and K^{*-} vector mesons with high precision. We observe the first non-zero spin alignment for $K^{*\pm}$ in heavy-ion collisions. The $K^{*\pm}$ ρ_{00} is larger than that of K^{*0} for 20–60% central isobar collisions. The current large deviation of $K^{*\pm}$ ρ_{00} and its ordering with K^{*0} is surprising, and opposite to the naive expectation from B-field. These results pose challenges to current understanding and inputs from theory are required to interpret the ρ_{00} results from isobar data.

REFERENCES

[1] F. Becattini *et al.*, *Phys. Rev. C* **77**, 024906 (2008).

[2] Z.T. Liang, X.N. Wang, *Phys. Lett. B* **629**, 20 (2005).

[3] D. Kharzeev *et al.*, *Nucl. Phys. A* **803**, 227 (2008).

[4] STAR Collaboration (L. Adamczyk *et al.*), *Nature* **548**, 62 (2017); STAR Collaboration (J. Adam *et al.*), *Phys. Rev. C* **98**, 014910 (2018).

[5] K. Schilling *et al.*, *Nucl. Phys. B* **15**, 397 (1970).

[6] Y.G. Yang *et al.*, *Phys. Rev. C* **97**, 034917 (2018).

[7] X.L. Xia *et al.*, *Phys. Lett. B* **817**, 136325 (2021); J.H. Gao, *Phys. Rev. D* **104**, 076016 (2021); B. Müller, D. Yang, *Phys. Rev. D* **105**, L011901 (2022).

[8] X. Sheng *et al.*, *Phys. Rev. D* **101**, 096005 (2020); *ibid.* **102**, 056013 (2020); arXiv:2206.05868 [hep-ph]s.

[9] STAR Collaboration (M.S, Abdallah *et al.*), *Phys. Rev. C* **105**, 014901 (2022).

[10] STAR Collaboration (B.I. Abelev *et al.*), *Phys. Rev. C* **79**, 034909 (2009).

[11] A.M. Poskanzer, S.A. Voloshin, *Phys. Rev. C* **58**, 1671 (1998).

[12] A.H. Tang *et al.*, *Phys. Rev. C* **98**, 044907 (2018).

[13] STAR Collaboration (M. Abdallah *et al.*), arXiv:2204.02302 [hep-ph].